ELSEVIER

Journal of Magnetism and Magnetic Materials 159 (1996) 269–281

journal of magnetism and magnetic materials

Giant magnetoresistance in granular cobalt copper thin films prepared by pulsed laser ablation deposition

T.J. Jackson [a,*], S.B. Palmer [a], H.J. Blythe [b], A.S. Halim [c]

[a] *Physics Department, University of Warwick, Coventry CV4 7AL, UK*
[b] *Physics Department, Hicks Building, University of Sheffield, Sheffield S3 7RH, UK*
[c] *Department of Physics, Universiti Pertania Malaysia, 43400 Serdang, Selangar, Malaysia*

Received 23 October 1995

Abstract

Giant magnetoresistance of up to 9.5% in 1.5 T at 14 K has been observed in $Co_{19}Cu_{81}$ thin films prepared by pulsed laser ablation deposition from rotated, split targets. The as-grown films show a small GMR effect but this may be enhanced by a factor of 4 by appropriate annealing. The volume ratio of material in the target is found to be reproduced in the film. Measurements of the remanence and initial susceptibility of the films indicate a distribution of energy barriers to the rotation of the magnetic moments of the cobalt particles and also the presence of inter-particle interactions. The choice of operating parameters to control these effects and thus optimise the GMR is discussed.

Keywords: Giant magnetoresistance; Pulsed laser ablation deposition

1. Introduction

There has been a great deal of interest in granular thin films displaying the giant magnetoresistance (GMR) effect. Granular systems are interesting from an applications perspective because the magnetoresistance is essentially isotropic and the films are much simpler to prepare than multilayers. In the cobalt copper system of interest to the present work, a GMR ratio defined by

$$\Delta R/R_{\min} = \left[\left(R(B) - R_{\min}\right)/R_{\min}\right] \quad (1)$$

of up to 20% has been observed in sputtered $Co_{20}Cu_{80}$ films in applied fields up to 0.5 T at low temperatures by, for example, Berkowitz et al. [1] and Xiao et al. [2]. $R_{\min}$ is either the value of the resistance at saturation or else the value of the resistance in the highest field available in the laboratory.

At equilibrium there is almost no solubility of cobalt in copper and only a small solubility of copper in cobalt [3]. However, metastable face centred cubic (fcc) alloys may be obtained by, for

* Corresponding author. Present address: Materials Science and Metallurgy, University of Cambridge, Pembrooke Street, Cambridge CB2 3QZ, UK. Fax: +44-1223-334373; email: tjj29@cus.cam.ac.uk.

SSDI 0304-8853(95)00648-6

example, evaporation or sputter deposition onto low temperature substrates as shown by Childress and Chien [4] and earlier by Kneller [5]. If such a film is annealed at elevated temperatures then phase separation occurs, the cobalt particles precipitating out from the copper matrix in accordance with the phase diagram. Thus, it is normal for the magnetoresistance in granular films to be increased by annealing which increases the size of the cobalt precipitates. If the particles become too large then the GMR is degraded. For example, the films prepared in [2] showed a GMR of 18% at low temperatures after a 10 min anneal at 500°C, but an alternative anneal for 10 min at 650°C resulted in a reduced GMR of 8%. For high magnetoresistance the non-magnetic matrix (in this case copper) must be 'clean'; the presence of isolated cobalt atoms between the particles responsible for the GMR will cause spin-flip scattering which degrades the magnetoresistance [6]. However, the size of the cobalt precipitates and the separation of the precipitates must be smaller than the spin-dependent mean free path. In the cobalt copper (CoCu) system, a mean free path of the order of 5 nm in the magnetic particles and 25 nm in the non-magnetic matrix has been estimated [7]. In addition, the cobalt precipitates should be small enough to be single magnetic domains.

More recently Huai et al [8] have reported a GMR of up to 8% in 1 T in films prepared by pulsed laser ablation deposition (PLAD). However, in this paper no mention was made of the magnetic properties of the films. In the present paper we corroborate the reported level of GMR in CoCu films prepared by the PLAD technique and also correlate the magnetic properties of the films with the magnetoresistance.

The highest observed GMR in the CoCu system is lower than that which may be achieved in other granular systems, for example cobalt–iron alloy in silver [9]. This may be due in part to the small solubility of copper in cobalt as discussed by Dieny [10]; a concentration gradient at the surface of the cobalt precipitates may result in a non-ferromagnetic shell around the core of the precipitate and degrade the magnetoresistance. However, the number ratio of cobalt to copper atoms deposited on the substrate after ablation from a split target closely matches the cobalt to copper volume ratio in the target, a simplification which makes the CoCu system attractive for an initial study. Measurements of the deposition rate of a variety of metals using an in situ quartz crystal microbalance have shown that this is not true for all metals with, for example, silver being deposited much more rapidly than cobalt.

2. Preparation

UV radiation from a XeCl excimer laser (wavelength 308 nm, pulse length 30 ns, repetition rate 9 Hz) was focused onto a split CoCu target at an angle of incidence of 45°. The target was contained in a stainless-steel vacuum chamber evacuated to a pressure $\sim 10^{-6}$ mbar. The split target, shown in Fig. 1, comprised of a disc with cobalt and copper sectors in proportions appropriate to the desired film composition of around 25% Co. The first of the two films described here, sample 1, was grown with the target rotated with a period of 6 s. Sample 2 was grown with the target rotated with a period of 1 s. The feedthrough used to provide this rotation was of the O-ring sealed type; faster rotation led to a degradation of the vacuum quality. The laser was set to produce an energy per pulse of 100 mJ and the beam was focused to a spot size of 3 mm^2 at the target, as measured from the total area of a stationary target affected by the laser beam. The target and substrate were 4 cm apart and the plume stopped just short of the substrate. Prior to deposition, the targets were cleaned with 2000 laser pulses while a shutter was held over the substrate. The films were deposited onto de-greased Si substrates which were placed parallel to the target and held at room temperature. Both films were grown using 40000 laser pulses. After growth the films were each divided into three parts. Parts 1a and 2a underwent no further treatment. Parts 1b and 2b were annealed for 15 minutes

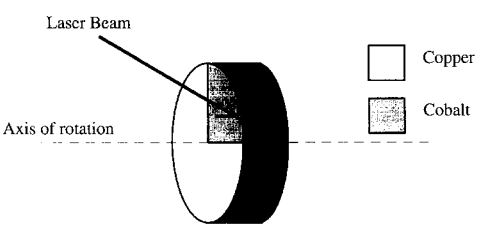

Fig. 1. The split cobalt/copper target.

at 290°C and parts 1c and 2c were annealed for 10 min at 457°C. These annealing strategies were chosen as consistent with the optimum strategies reported in other work (see, for example, [1], [2] and [8]). All of the anneals were carried out in the deposition chamber at 10^{-6} mbar using a heater described elsewhere [30]. The sample temperature was measured with a thermocouple bolted to the backing plate on which the substrate was mounted.

3. Experimental method

3.1. Surface morphology

The surfaces of the films and targets after ablation were examined in the scanning electron microscope (SEM).

3.2. Composition, thickness and structure

Energy dispersive X-ray analysis, also in the SEM, was used to determine the overall composition of the films to within an accuracy of approximately 5%. The thickness of the films was measured to an accuracy of ± 20 nm with a stylus instrument. The crystalline state of the films was determined by X-ray diffraction using Cu K_α radiation in a θ–2θ powder diffractometer.

3.3. Magnetoresistance

Some GMR systems exhibit a hysteresis on cycling the applied magnetic field, with the maximum resistance, R_{max}, occurring not in zero applied field but in a field equivalent to the coercive field of the magnetic hysteresis loop. Furthermore, not all samples show a saturation of the magnetoresistance in the highest field available in the laboratory. It is therefore preferable to quantify the magnetoresistance in the traditional way [11]:

$$\Delta R/R_{max} = \left[\left(R(B) - R_{max}\right)/R_{max}\right] \times 100. \quad (2)$$

Scattering of the conduction electrons by impurities and defects increases R_{max} and can mask the change in resistance $(R(B) - R_{max})$ due to the ordering influence of the applied magnetic field. Such scattering mechanisms are expected to be temperature independent. Thermal activation acts against the field-induced order and so $(R(B) - R_{max})$ is expected to be larger at low temperatures. In addition scattering by phonons is also reduced at low temperatures, providing further increases in the measured magnetoresistance.

The two definitions given by Eqs. (1) and (2) are related by [10]

$$\Delta R/R_{min} = |\Delta R/R_{max}|/\left(|\Delta R/R_{max}| - 1\right). \quad (3)$$

In the present work dc resistance measurements were made in a continuous flow cryostat to an accuracy of $\pm 0.1\%$ with a resolution of 1 mΩ by a standard four-point probe method. Contacts to the samples were made using silver dag. Since the samples were sub-divisions of the original, as-grown films, they were too small for the usual conversion of electrical resistance to sheet resistivity ($R_s = 4.53$ V/I) to be applied. This conversion requires the sample to be equivalent to a semi-infinite sheet. Therefore the results are presented in terms of the measured resistance only. The magnetic field was applied in the plane of the film and parallel to the direction of the current. The magnitude of the applied field was measured with a Hall probe placed alongside the cryostat.

3.4. Magnetic properties

Magnetic measurements were performed in a SQUID magnetometer. The magnetic field was applied parallel to the plane of the film. The initial (dc) susceptibility was measured by cooling the sample to 5 K in zero applied field and recording the magnetic moment of the sample on warming in a small (5 mT) applied field. This measurement is termed the zero field cooled (ZFC) curve. Then the sample was cooled in the same field, yielding the field cooled (FC) curve. The remanence of the sample was measured with increasing temperature after cooling from room temperature in zero applied field. A saturating field (in this case a field of 5 T) is applied to the sample at 5 K and the remanent moment measured approximately 100 s after settling at each measurement temperature.

These measurements were chosen since they are appropriate to the characterisation of an assembly of ferromagnetic particles displaying superparamagnetic

behaviour [12], as expected for the cobalt precipitates in these films. Superparamagnetism occurs when the thermal energy, $k_B T$, is comparable with the total anisotropy energy of a ferromagnetic domain of volume V_p, the anisotropy energy providing the energy barrier in the activation process. There is a characteristic relaxation time, τ, for the decay of the remanence given by

$$\tau^{-1} = 2\upsilon_0 \exp(-KV_p/k_B T), \tag{4}$$

where υ_0 is an attempt frequency and K the anisotropy constant which in general will include contributions from both the crystalline and the shape anisotropy. Taking a typical dc measurement time $t = 100$ s such that $(t/\tau) > 1$ produces the well-known criterion for the 'blocking temperature', T_B, above which superparamagnetism occurs and below which the particle behaves as a conventional ferromagnetic single domain:

$$25k_B T_B = KV_p. \tag{5}$$

Above T_B the remanence should be zero as the particles achieve thermal equilibrium within the measurement time. In any real assembly of small particles there will be a distribution of particle sizes and thus a distribution of blocking temperatures, T_B. The temperature differential of the remanence gives a measure of the distribution of energy barriers and thus, in the absence of inter-particle interactions, of the distribution of blocking temperatures in the assembly.

The initial (dc) susceptibility as measured by the ZFC curve reaches a maximum at a temperature, T_f, corresponding to the blocking temperature of particles of average size. The rise in the magnetisation on warming from low temperatures is due to the increased susceptibility of the assembly, as the fraction of particles becoming unblocked and showing superparamagnetic behaviour increases. The magnetisation peaks and subsequently falls on continued warming due to the disordering influence of thermal activation. Ideally, far above the highest blocking temperature T_B of the assembly, the ZFC curve is reversible and follows a Curie-like $1/T$ law. However on subsequent cooling towards T_f (the FC measurement) the magnetisation rises above the ZFC curve as T_f is approached. If only a single particle size were present, then this separation or bifurcation would occur at T_f. In a real assembly the bifurcation occurs at a temperature $T_b > T_f$ corresponding to the blocking temperature of the largest particles in the assembly. The FC magnetisation saturates at low temperatures below T_b and T_f.

The hysteresis loops of samples 1a and 2c were also measured at various temperatures. The diamagnetic contribution of the substrate was determined from the high field susceptibility and subtracted from the data. An assembly of non-interacting superparamagnetic particles should show no hysteresis and curves of magnetisation, M, versus B/T, where B is the applied magnetic field and T the measurement temperature, should be universal.

4. Results and discussion

4.1. Surface morphology

Observation of the surfaces of the films in the SEM showed droplets splashed from the targets during the ablation. A representative photograph of the surface of the film sample 1a is shown in Fig. 2. If the electron beam is focused onto a region of interest instead of scanned across the sample, it is possible to analyse the composition of sections of the film regions approximately 1 μm^2 in area, this being the region within the sample from which X-rays are detected. No droplets of mixed composition were expected and none were recorded. The largest

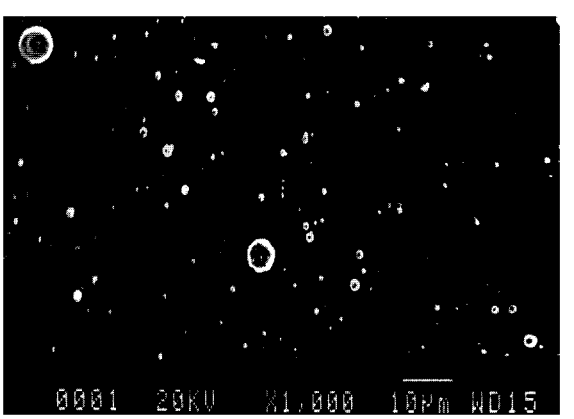

Fig. 2. SEM photograph of the surface of sample 1a showing the broad distribution of the sizes of the droplets.

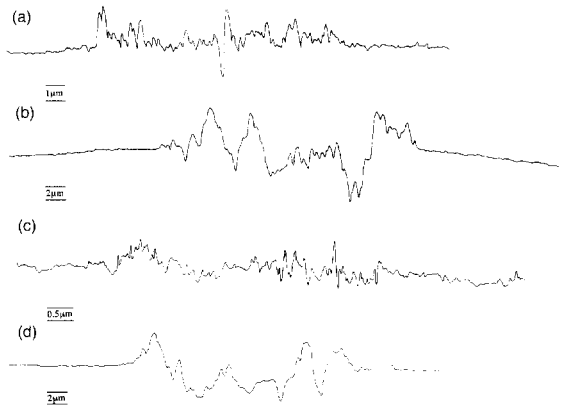

Fig. 3. Cross sections across the minor axis of the holes cut by the laser beam into stationary targets. (a) Copper after 1 pulse. (b) Copper after 50 pulses. (c) Cobalt after 1 pulse. 3d: Cobalt after 50 pulses. The horizontal magnification on all four traces is 200×.

droplets with diameters in the range 4–20 μm were almost exclusively cobalt, while over 90% of the droplets with diameters less than 4 μm were copper. The as-grown films were 1 cm^2 in area; taking the mean value of the thickness of 200 nm gave a volume of material within the body of the film of the order of $(2.0 \pm 0.2) \times 10^{-5}$ cm^3. Using the numerical data for the composition of the droplets given above it was found that the ratio of the volume of cobalt and copper deposited as droplets was the same as that in the underlying films. The composition analysis remained unchanged if taken over a large area such as that recorded in Fig. 2 or by focusing the electron beam down to a spot aimed between the droplets. The volume of copper deposited as droplets was estimated to be similar to the total volume deposited as film material, namely 2×10^{-5} cm^3; the total volume of cobalt droplets was approximately a factor of 5 smaller.

The relative rates at which material was removed from the target in vapour and liquid form was investigated by ablating individual cobalt and copper targets under conditions identical to those used for the films' deposition, except that the targets were not rotated. The lack of rotation allowed a single, well defined hole, the volume of which could be estimated by surface profiling, to be cut into each target. Fig. 3 shows surface profiles across the minor axis of the hole cut into the targets by the laser beam after 1 and 50 laser pulses. Irregular ridges of material are seen which presumably arise from the recoil momentum of the plume acting on the molten surface during the time within the length of the laser pulse that the surface temperature is above the melting point. It is not expected that this recoil momentum, acting as a 'piston' on the melt, is the source of the splashing of droplets. The radial velocity required to carry the melt out from under the laser spot is given by w/τ_p, where w is the area from which significant material removal has occurred and τ_p is the pulse length [13]. This is several orders of magnitude larger than the droplet velocity measured in time-of-flight experi-

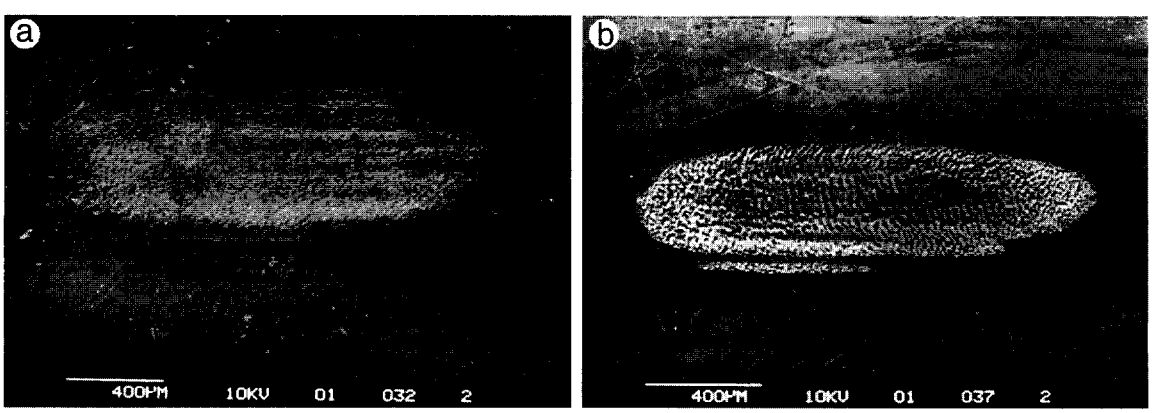

Fig. 4. SEM photographs of the laser induced surface structure on a stationary copper (a) and cobalt (b) target after 50 pulses. The photographs indicate the spot size of the laser beam at the target and highlight the differences in the induced strucuture on copper and cobalt.

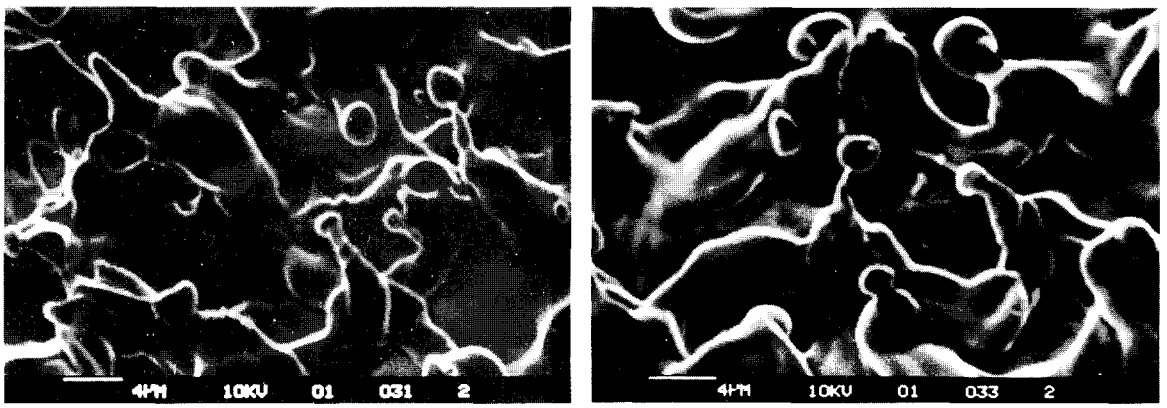

Fig. 5. Close-up views of the hole cut into the copper target after 50 pulses.

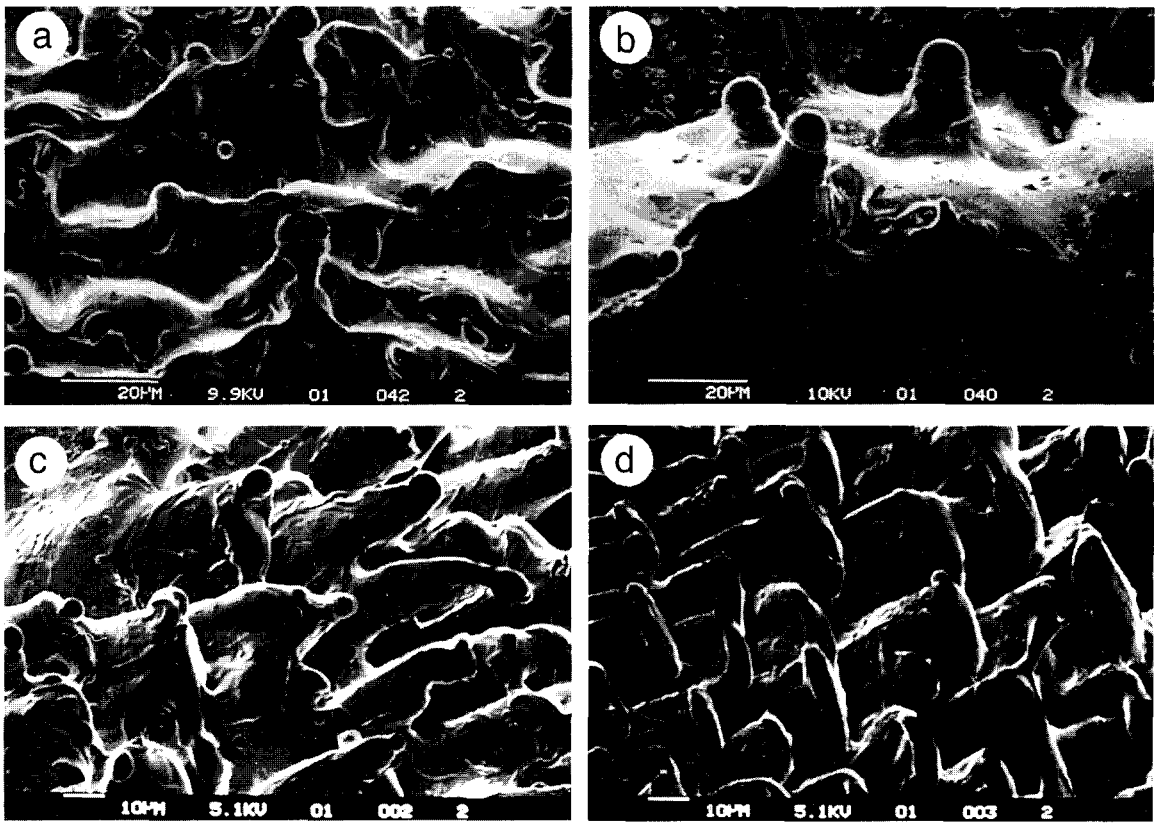

Fig. 6. Close-up views of the hole cut into the cobalt target. (a) Ridges across the width of the spot viewed from the back after 50 pulses. (b) Asperities on the top of a columnar structure after 50 pulses. (c) Cones at the front of the hole after 100 pulses. (d) Columns at the back of the hole after 100 pulses.

ments [14]. Although the laser beam causes a clearly visible modification of the surface of the target approximately 3 mm^2 in area, the hole cut into the target from which most of the material is removed is of the order of 1 mm^2 in area. Fig. 4 shows SEM photographs of the surfaces of the copper and cobalt targets respectively after 50 laser pulses demonstrating this effect, which arises from the non-uniformity of the excimer laser beam. Fig. 4a and Fig. 4b also indicate the different surface structures induced by the laser beam on copper and cobalt. The damage on copper is uniform throughout the spot – close-up views are presented in Fig. 5a and Fig. 5b – and has been observed to show little change whether the number of pulses is of the order of 10 or 10^3. Droplets frozen in the act of emission from extended asperities may be seen clearly. In contrast, on cobalt the features at the front and back of the spot appear smaller in lateral dimensions than those in the centre. The differences may arise from thermal gradients across the spot during the laser pulse. Closer analysis shows the presence of 'cones' and 'columns' at the front and back and 'ridges' in the centre. Fig. 6a shows the ridges viewed from the back of the spot; the ridges run from right to left. Rounded asperities larger than those seen on copper are concentrated at the edges of the ridges. Similar asperities also arise on the tops of the columns, as shown in Fig. 6b. The presence of larger features on the surface of the cobalt target than on the copper target correlates well with the sizes of the droplets observed on the films. Fig. 6c and d show the cones and columns at the front and back of the spot on cobalt after 100 pulses. After continued ablation the ridges are cut into columns and eventually removed completely producing a narrow, deep and jagged-edged hole. It has been observed that the plume above a cobalt target narrows and weakens on continuous ablation much more rapidly than that above copper, an effect which may be attributed to the 'channelling' of the plume by the deep hole.

Table 1
Melting points of metals of interest to this work [18]

Metal	Melting point, T_{mpt} (K)
Cobalt	1765
Copper	1356
Silver	1234
Nickel	1726
Iron	1808
Niobium	2741

Table 2
Parameters used for the evaluation of Eqs. (4) and (5). Data from Refs. [18–22]. Room temperature values were used for the solid density and thermal expansion

Property	Cobalt	Copper
Maximum surface temperature, T_{max} (K)	2740	2740
Atomic mass (amu)	58.93	63.55
Solid density ρ_s ($kg\,m^{-3}$)	8900	8930
Heat of vapourisation, ΔH_v ($eV\,atom^{-1}$)	4.04	3.16
Liquid surface energy, γ ($J\,m^{-2}$)	1.9	1.3
$T_{max} - T_{mpt}$ (K)	975	1384
Thermal expansion, $\alpha(T_{max} - T_{mpt})$	0.012	0.024
Liquid density ρ_l ($kg\,m^{-3}$)	7740	8033

Experiments on other metals, including silver, nickel, iron and niobium, have shown that, at these laser irradiances, all of these materials undergo surface melting, although the melting of niobium is much less extensive. Table 1 gives the melting points of these metals. From these data, the maximum surface temperature may be crudely estimated as 2740 K if we make the assumption that the thermal and optical properties of all these metals are essentially the same under the intense laser irradiation. This assumption is consistent with the work of Kelly and Rothenberg [15], whose analysis we now follow, and the maximum temperature deduced is consistent with the measurements of Dreyfus [16] and Dyer [17].

The rate of thermal evaporation may be estimated using this value for the maximum surface temperature [15] by

$$\text{depth/pulse} = \left(p_m T_m^{1/2} \tau_p / M^{1/2} \Delta H_v \right) \times 1.53 \times 10^6 \text{ nm/pulse}, \quad (6)$$

where p_m is the vapour pressure in atmospheres at the maximum surface temperature T_m, M the atomic weight in atomic mass units and ΔH_v is the heat of vapourisation in units of eV/atom. Using data summarised in Table 2 and p_m equal to 0.7 atm for copper and 0.1 atm for cobalt [22], we find depths per pulse of the order of 8×10^{-3} nm for cobalt and 7×10^{-2} nm for copper. However, the plume from

the copper target was noticed to be much broader than that from the cobalt target, which is consistent with the observed deposition rates being similar. It is difficult to compare these rates quantitatively with the surface profiles of the holes cut by the laser owing to the roughness of the holes. However for 50 pulses a depth of 0.4 nm is predicted by Eq. (6) for cobalt i.e. a depth of the order of one monolayer. Therefore either the surface temperature T_m and thus p_m are far higher than expected or else the ablation is driven by other mechanisms and involves a substantial amount of material leaving the target in the liquid state.

Kelly and Rothenberg [15] have described a hydrodynamic process of droplet expulsion, in which droplets are expelled from the tips of asperities on the surface if the total momentum away from the substrate, due to the thermal expansion of the melt and the volume change on melting, exceeds the product of the surface tension force and the time within each laser pulse for which the surface is molten. It is easy to see from Figs. 3 and 4 how such asperities arise. Close-up photographs from inside the hole cut by the laser for cobalt and copper, shown in Figs. 5 and 6, confirm these asperities as sources of droplets. The size of the asperities is consistent with the sizes of the droplets observed on the films. From these arguments a minimum droplet radius r_{min} may be calculated [15]:

$$r_{min}^3 = \left\{3\gamma\tau_p^2\left(1 - T_{mpt}^2/T_{max}^2\right)^2\right\} / \left\{\rho_l\left(\alpha\left(T_{max} - T_{mpt}\right) + \left(\rho_s - \rho_l\right)/3\rho_s\right)\right\}. \quad (7)$$

Using the quantities in Table 2, Eq. (7) yields a minimum radius of 1.6 μm for both copper and cobalt, which again is consistent with experiment, but the size distribution is not addressed. This model for the evolution of droplets considers the droplets to arise at the surface of the target and not from subsurface heating as may be expected in the ablation of, for example, oxide superconductors. In these oxides the thermal diffusion length is much shorter than the optical penetration depth; the reverse in true in metals. The model does suggest that the use of picosecond laser pulses might afford a considerable advantage in terms of a reduction in the emission of droplets.

The base pressure of the vacuum system available (of the order of 10^{-6} mbar) necessitates the use of a high laser irradiance to achieve a deposition rate significantly higher than the impurity arrival rate. Unfortunately, this promotes droplet emission. By de-focusing the laser beam it is possible to reduce the droplet production sufficiently for the growth of thin layers suitable for multilayer structures. The surface quality of the films described in this article should not be taken as the limit of what may be achieved by the PLAD technique.

4.2. Composition, thickness and structure

Sample 1 had the nominal composition $Co_{19}Cu_{81}$ ($\pm 5\%$) and a thickness of 180 ± 20 nm; sample 2

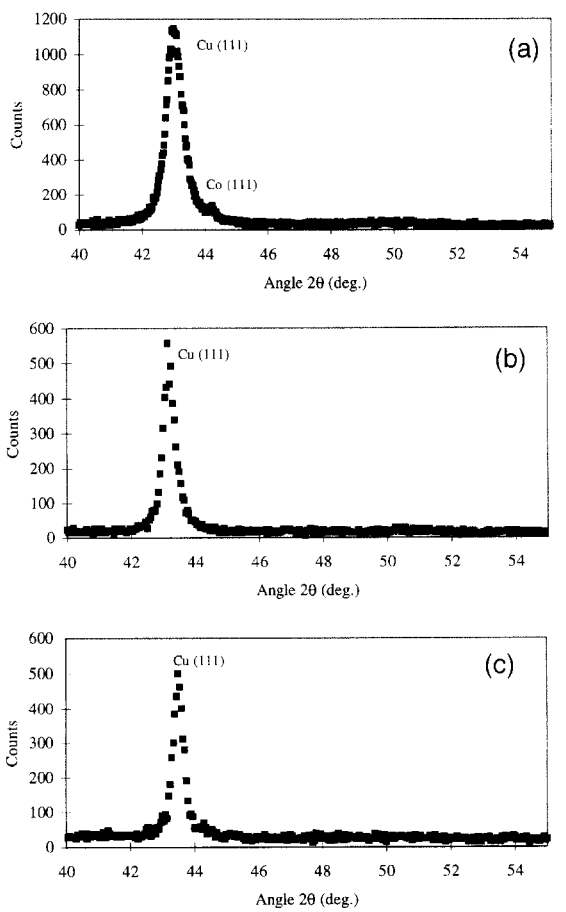

Fig. 7. X-ray diffraction data for samples 1a (a), sample 1b (b) and sample 1c (c).

had the composition $Co_{26}Cu_{74}$ ($\pm 5\%$) and a thickness of 220 ± 20 nm. Given the errors associated with these measurements the films were assumed to have grown with the same composition and at the same average rate of the order of 0.05 nm s^{-1}, which was slightly higher than the rate used in Ref. [8]. If the inter-atomic spacing is taken to be 0.3 nm then, in both cases, the growth rate corresponded to the deposition of roughly one monolayer every 6s, or after one rotation of the target for sample 1 and after 6 rotations for sample 2. Had a slower rotation rate been used then the film so produced might have grown with a 'rough' multilayer structure, which was not the object of these experiments.

The X-ray diffraction measurements on both sets of samples 1a, 1b and 1c and 2a, 2b and 2c were very similar. Fig. 7 shows the data for samples 1a and 1c. In a polycrystalline copper sample the peaks corresponding to the {111} and {200} planes at 43.2° and 50.5° should be present with relative intensities 100:46 over this angular range. The absence of the {200} peak evidences a high degree of texturing with the {111} planes lying parallel to the plane of the film. The texturing may arise from the growth rate, the {111} planes being the most densely packed planes in the fcc lattice [23]. Other films we have prepared under similar conditions, including granular cobalt silver (CoAg) and nickel, also show a tendency towards this texturing. CoCu films prepared by PLAD at a lower growth rate than that presented here showed less strong texturing [8]. The peak at 44.2° may be identified with the fcc cobalt {111} planes. The small size of this cobalt peak suggests that the Co particles are poorly crystallised, as has been observed in transmission electron microscopy (TEM) of CoAg films [24]. Shoulders on the copper peak are suggestive of some alloying at the interface between the cobalt particles and the copper matrix, as expected from the phase diagram.

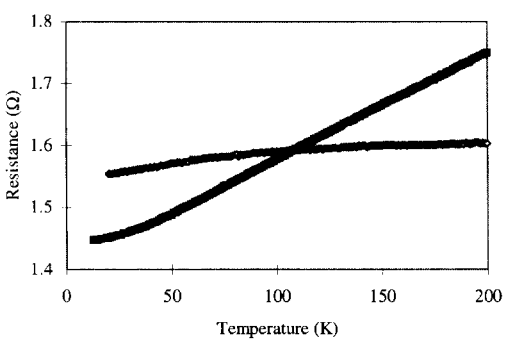

Fig. 8. Resistance versus temperature curves for the as grown films 1a and 2a. (◇) Sample 1a, (■) sample 2a

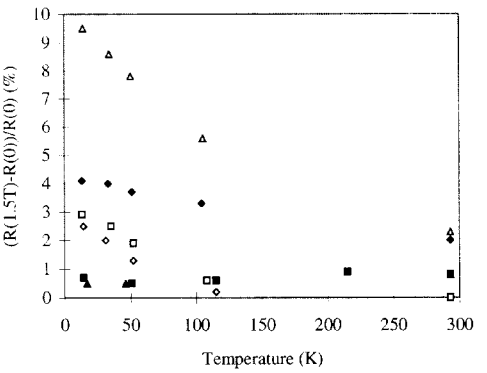

Fig. 9. Maximum magnetoresistance ratio versus temperature for all samples, showing the effect of annealing (increases the maximum magnetoresistance ratio). At low temperatures, thermally-induced disorder in the magnetic alignment and the scattering of the conduction electrons by phonons are reduced and so the observed magnetoresistance is higher. (◇) Sample 1a, (□) sample 1b, (△) sample 1c, (■) sample 2a, (▲) sample 2b, (◆) sample 2c.

In the as-grown film sample 1a, the copper peak is at 43.0°. This narrows and moves towards higher angles upon annealing, due to the relaxation of stress within the film and the removal of defects from the lattice structure during the annealing process. There was some splitting of the copper peak in the data of sample 2a, evidencing some metastable alloy phases produced during growth, which disappeared on annealing.

4.3. Magnetoresistance

The variation of the zero field resistance with temperature was measured for each sample. The resistance of samples 1a and 1b was found to be concave towards the temperature axis with a drop of only 2.8% between room temperature and low temperatures. This non-metallic behaviour can be attributed to 'impurity' scattering from defects within the lattice structure and grain boundaries. The resistance of sample 1c displayed more conventional metallic behaviour with a linear decrease of 20.6% between room temperature and 14 K. The resistance

of all three samples 2a, 2b and 2c showed a linear fall of the order of 25.0% on cooling. Illustrative data for samples 1a and 2a are shown in Fig. 8.

Sample 1a showed no magnetoresistance at room temperature but, upon cooling to 14 K, a magnetoresistance ratio $\Delta R/R_{max}$ of 2.5% was observed in 1.5 T. The low temperature anneal (sample 1b) made little difference to the transport properties. A GMR of 2.3% at room temperature and 9.5% at 14 K was recorded in sample 1c, the sample subjected to the high temperature anneal. The GMR in all versions of sample 2 was always smaller than that in the equivalent versions of sample 1. At 14 K a GMR of 4.5% was observed for sample 2c. The variation of the magnitude of the maximum magnetoresistance with temperature for all six samples 1a, 1b, 1c, 2a, 2b and 2c is shown in Fig. 9. Plots of $\Delta R/R$ versus field at room temperature and at 14 K for sample 1c and also sample 2c, are shown in Fig. 10. The resistance just saturated at high fields and no hysteresis was resolved on cycling the applied field.

The high temperature anneal produced an increase in the maximum magnetoresistance of 1c compared with 1a. This may be ascribed partly to the modification of the magnetic structure (growth of ferromagnetic precipitates) and partly to the improvement in the lattice structure. There are two reasons why the magnetoresistance is less at room temperature than at low temperatures: thermal activation acts against the ordering influence of the applied magnetic field and scattering by phonons is more significant. A strong

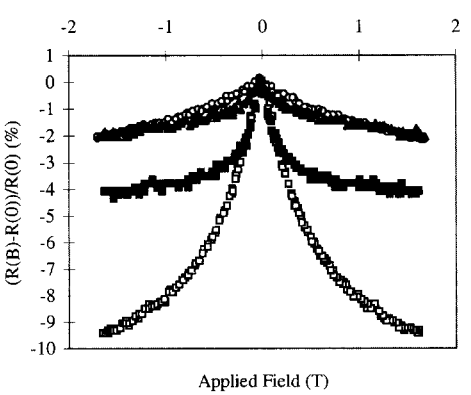

Fig. 10. Magnitude of the magnetoresistance of samples 1c and 2c at room temperature and at 14 K. (□) Sample 1c, 14 K; (○) sample 1c, 293 K; (■) sample 2c, 14 K; (▲) sample 2c, 293 K.

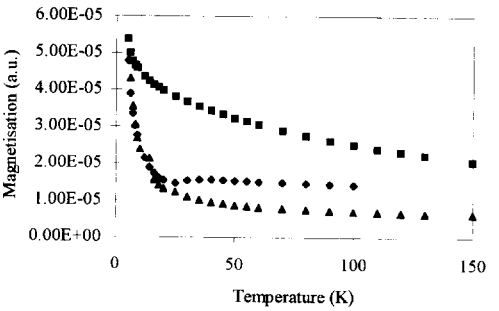

Fig. 11. Temperature dependence of the remanence of samples 1a, 1b and 1c normalised to the remanence at 5 K, showing the increases in the average blocking temperature T_B after annealing. (◆) Sample 1a, (▲) sample 1b, (■) sample 1c.

temperature dependence in R_{max}, aided by a reduction of 'parasitic' scattering of electrons by grain boundaries and lattice defects, contributes to the increase in the magnetoresistance at low temperatures.

It is instructive to compare the differences in behaviour between samples 1a and 1c and samples 2a and 2c. The similarity of the behaviour of the zero field resistance with temperature for samples 2a and 2c suggests that the differences in the magnetoresistance must be explicable mainly in terms of changes in the magnetic structure alone. More severe annealing (higher temperatures or longer times at 457°C) was found to lead to the formation of metal silicates due to a reaction between the film and the substrate.

4.4. Magnetic properties

Fig. 11 shows the temperature dependence of the remanence for samples 1a, 1b and 1c. The remanence is normalised to the value at 5 K. (The apparent minimum in the remanence of sample 1a is believed to be an experimental artifact since it is inconsistent with theories assuming an energy barrier distribution.) Two features are immediately noticeable in the data: the remanence remains finite at high temperatures and the mean blocking temperature, T_B, as defined in Eq. (5), increases after annealing (samples 1b and 1c). These observations suggest that (i) the samples are not truly superparamagnetic (indeed no scaling of magnetisation with reduced temperature was observed) and (ii) the size distribution of

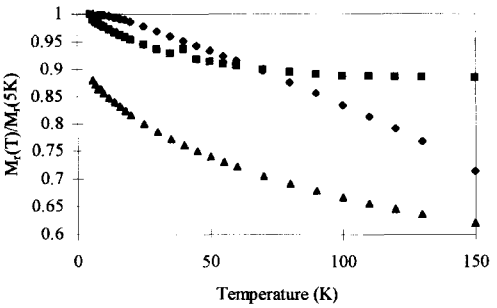

Fig. 12. Temperature dependence of the remanence normalised to the remanence at 5 K. (♦) Sample 2a, (▲) sample 2b, (■) sample 2c.

the cobalt precipitates is increased by the annealing as expected. Furthermore, the temperature differential of the remanence curve provides no evidence for a bi-modal distribution of blocking temperatures as is seen in some sputtered films [25]. Such a distribution may arise if the film is grown within the sputtering plasma plume, the plume providing sufficient thermal energy to partially anneal the film as it grows. Subsequent annealing removes the bi-modality from the distribution of blocking temperatures. The films reported here were grown outside the plasma plume and the substrate remained at room temperature during the deposition. Similar conclusions may be drawn from the remanence curves of samples 2a, 2b and 2c which are shown in Fig. 12.

It is tempting to use Eq. (5) to convert the mean blocking temperatures, T_B, from Figs. 11 and 12 into particle sizes. For example, samples 1a and 1b, with blocking temperatures of 25 K and 50 K respectively, yield mean particle sizes of 3.4 and 4.2 nm. Here we have used $|K_2| = 43 \times 10^4\ \mathrm{J\,m^{-3}}$ for fcc cobalt [26]. However, there are problems with such estimates. The bulk anisotropy constants are highly temperature dependent. Furthermore, shape anisotropy, which is expected to become more significant after annealing and also the effects of alloying at cobalt/copper interfaces, which will reduce the crystalline components to the anisotropy, are ignored. Rodbell [27] and Becker [28] observed that on annealing samples of 2% cobalt in copper the cobalt particles changed shape from spherical to ellipsoidal and that the anisotropy energies were reduced compared with the bulk values. Thus estimates such as those above are likely to underestimate the volumes of the particles. Nevertheless, the sizes we have deduced are slightly higher than the 2–3 nm reported for the particles in high GMR sputtered CoAg and CoFeAg films [9,23,24,29]. The surest, direct magnetic measurement yielding the particle size distribution would appear to be the fitting of Langevin functions to the universal M versus B/T curves from truly superparamagnetic samples, as in Ref. [29].

Low temperature (5 K) measurements of the M versus B curves for samples 1a and 2c showed that magnetic saturation was achieved in 0.5 T. The continuing change in resistance in fields at which magnetic saturation is already achieved suggests the presence of very small magnetic particles making a

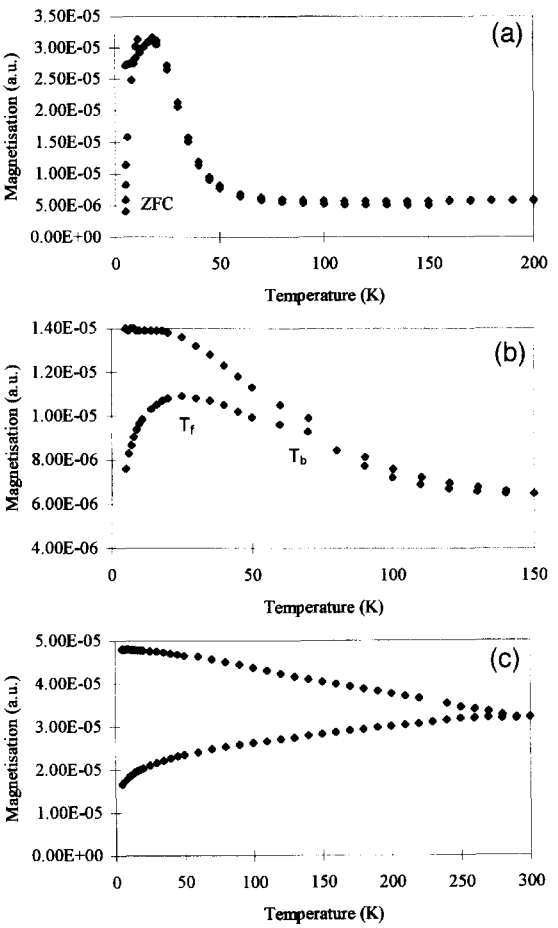

Fig. 13. Zero field cooled (ZFC) and Field cooled (FC) magnetisation curves for (a) sample 1a, (b) sample 1b and (c) sample 1c.

minor contribution to the magnetoresistance and a negligible contribution to the overall magnetisation. Since there is no 'tail' in the magnetoresistance at high fields, we may assume that all the magnetic particles eventually become aligned. The M versus B curves were found to be slightly hysteretic (although any hysteresis in the magnetoresistance was smaller than the resolution of the resistance measuring apparatus) and no universality was observed in curves of M plotted against B/T. These deviations from pure superparamagnetic behaviour may have several sources, including interparticle-interactions, alloying and of course the contribution of the cobalt droplets to the magnetisation.

The cobalt droplets, 4–20 μm in diameter, would be expected to show bulk ferromagnetism rather than superparamagnetic behaviour. Thus they probably made a major contribution to the background remanence seen in Figs. 11 and 12 while the blocking temperature T_B deduced will have been indicative of the cobalt-rich precipitates within the body of the underlying film. Future work will be based on films grown in a deposition system in which a higher vacuum is attainable. This will allow lower laser fluences to be used, leading to a lower ablation rate (and growth rate) and thus the avoidance of droplets.

The distribution of energy barriers may also be examined from the ZFC and FC initial (dc) susceptibility curves. Data for samples 1a, 1b and 1c, which are representative, are shown in Fig. 13 and for sample 2a in Fig. 14. For sample 1a, T_f and T_b coincide at 20 K, suggesting a narrow distribution, but the FC susceptibility shows a negative temperature coefficient below 20 K. Such behaviour in the FC at low temperatures is indicative of spin glass

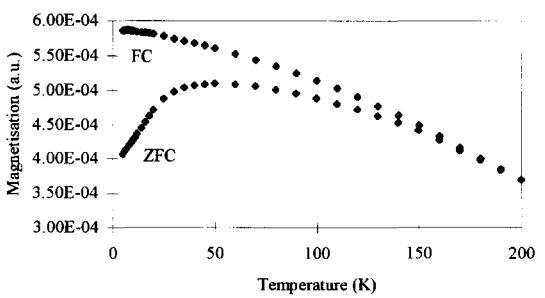

Fig. 14. Zero field cooled (ZFC) and Field cooled (FC) magnetisation curves for sample 2a.

Table 3
Characteristic temperatures deduced from the remanence (T_B) and ZFC and FC curves (T_f and T_b). '–' indicates that the temperature concerned is too close to, or above, the maximum measurement temperature of 300 K to be determined unambiguously

Sample	1a	1b	1c	2a	2b	2c
T_B (K)	25	50	–	–	–	–
T_f (K)	20	30	–	50	–	–
T_b (K)	20	70	–	150	–	–

behaviour due to alloying [4]. In sample 1b, T_f and T_b are increased and also separated; $T_f = 30$ K and $T_b = 70$ K. The FC susceptibility now shows a positive temperature coefficient at low temperatures. Table 3 summarises the broadening of the distribution, the increase in the mean and maximum blocking temperatures (T_f and T_b respectively) and additionally the separation of T_f and T_b from T_B observed in samples 1a, 1b and 2a, the samples where these temperatures were well defined. The results are consistent with an increase in the sizes of the particles on annealing as expected, leading to an increased magnetoresistance effect. Again the weakly temperature dependent magnetisation at higher temperatures towards room temperature is probably due to the cobalt droplets. For samples 1c, 2b and 2c the highest measurement temperature (300 K) was too low in order to provide clear, unambiguous data for T_f and T_b, as might be expected from the remanence curves of Fig. 12.

The faster rotation of the target during the growth of film 2 seems to have led to higher energy barriers for the rotation of the magnetic moments of the cobalt particles and also a lower magnetoresistance effect compared with sample 1. The origins of the energy barriers lie in the size, shape and crystal perfection of the particles, as well as in interaction effects, and will also be influenced by alloying. These conclusions suggest that a TEM study would be useful in future studies.

Variation of the laser irradiance at the target provides some means of control of the sizes of the magnetic particles [8] in the as-grown films. At high irradiances, clusters of atoms may be ablated from the target. In addition, diffusion of the atoms on the substrate will be encouraged if the atoms are arriving with high kinetic energies. Thus the cobalt precipitates in the as-grown film might become too large

for an optimised magnetoresistance effect. These observations provide a tentative explanation of the lower GMR observed to date in films prepared by PLAD than in sputtered films. Sputtering, in contrast to PLAD, is always an atomistic process. The remanence data in Ref. [25] also suggests that there may be fewer large magnetic particles in the as-grown sputtered films; the GMR effect is enhanced on annealing as the particle size distribution shifts upwards towards the optimum, but particles with dimensions greater than the spin-dependent mean free path will degrade the magnetoresistance.

5. Conclusions

We have confirmed that GMR close to 10% in 1.5 T at low temperatures may be observed in granular CoCu thin films prepared by PLAD from rotated, split targets. The magnitude of the magnetoresistance is dependent upon the distribution of energy barriers to the rotation of the magnetic moments of the cobalt particles. This distribution may be influenced by the growth parameters, including the laser irradiance at the target, a low irradiance being advisable and also by the ratio of the rate of rotation of the target to the growth rate.

Acknowledgements

This work has been aided considerably by technical support from Mr. J. Reed, who built the quartz crystal microbalance system, Mr. M.J. Cooper (assistance with the laboratory), Mr. D. Lee (target preparation) and Mr. S. York and Mr. G. Smith (electron microscopy). The programme on pulsed laser ablation deposition of metallic magnetic materials at Warwick is funded by the UK EPSRC. Dr. Halim acknowledges support from the Malaysia 6th Plan.

References

[1] A.E. Berkowitz, J.R. Mitchell, M.J. Carey, A.P. Young, S. Zhang, F.E. Spada, F.T. Parker, A. Hutten and G. Thomas, Phys. Rev. Lett. 68 (1992) 3745.
[2] J.Q. Xiao, J.S. Jiang and C.L. Chien, Phys. Rev. Lett. 68 (1992) 3749.
[3] M. Hansen, Constitution of Binary Alloys (McGraw Hill, New York, 1958) p. 5320.
[4] J.R. Childress and C.L. Chien, Phys. Rev. B 43 (1991) 8089.
[5] E. Kneller, J. Appl. Phys. 33 (1962) 1358.
[6] G.A. Gehring, J.F. Gregg, S.M. Thompson and M.L. Watson, J. Magn. Magn. Mater. 140–144 (1995) 501.
[7] S. Zhang, Appl. Phys. Lett. 61 (1992) 1853.
[8] Y. Huai, M. Chaker, H. Pépin, S. Boily, X. Bian and R.W. Cochrane, J. Magn. Magn. Mater. 136 (1994) 204.
[9] C. Bellouard, B. George and G. Marchad, J. Phys.: Condens. Matter 6 (1994) 723.
[10] B. Dieny, J. Magn. Magn. Mater. 136 (1994) 335.
[11] L.F. Bates, Modern Magnetism (Cambridge University Press, Cambridge, 1961) p. 363.
[12] M. El-Hilo, K. O'Grady and R. Chantrell, J. Magn. Magn. Mater. 117 (1992) 21.
[13] M. Von Allmen, Laser-Beam Interactions with Materials (Springer, Berlin, 1987) p. 168.
[14] H. Dupendant, J.P. Gavignan, D. Givord, A. Lienard, J.P. Rebouillat and Y. Souche, Appl. Surf. Sci. 43 (1989) 369.
[15] R. Kelly and J.E. Rothenberg, Nucl. Instr. and Meth. B 7/8 (1985) 755.
[16] R.W. Dreyfus, J. Appl. Phys. 69 (1991) 1721.
[17] P.E. Dyer, Appl. Phys. Lett. 55 (1989) 1630.
[18] R.M. Tennent, Science Data Book (Oliver and Boyd, Edinburgh, 1971) pp. 56–58.
[19] L.E. Muir, Interfacial Phenomena in Metals and Alloys (Addison Wesley, London, 1975) p. 101.
[20] A.F. Crawley, Int. Metall. Rev. 19 (1974) 32.
[21] Y.S. Touloukain, R.K. Kirby, P.E. Taylor and P.D. Desai, Thermophysical Properties of Materials, Vol. 12: Thermal Expansion, Metallic Elements and Alloys (IFC/Plenum, New York, 1975) pp. 71–79.
[22] D.R. Lide, ed., CRC Handbook of Chemistry and Physics (CRC Press, Boca Raton, 1992) pp. 4122–4146.
[23] A. Maeda, M. Kume, S. Oikawa, Y. Shimizu and M. Doi, J. Phys.: Condens. Matter 5 (1993) 4641.
[24] Z.C. Li, H. Wan, J. Liu, A. Tsoukatos, G.C. Hadjipanayis and L. Liang, Appl. Phys. Lett. 63 (1993) 3011.
[25] S.J. Greaves, M. El-Hilo, K. O'Grady and M. Watson, J. Appl. Phys. 76 (1994) 6802.
[26] R.S. Tebble and D.J. Craik, Magnetic Materials (Wiley Interscience, London, 1969) p. 72.
[27] D.S. Rodbell, J. Appl. Phys. 29 (1958) 311.
[28] J.J. Becker, J. Appl. Phys. 29 (1958) 317.
[29] S.M. Thompson, J.F. Gregg, C.R. Staddon, D. Daniel, S.J. Dawson, K. Ounadjela, J. Hammann, C. Fermon, G. Saux, K. O'Grady, S.J. Grieves, J.M.D. Coey and A. Fagan, Philos. Mag. B 68 (1993) 923.
[30] N.J. Appleyard, T.J. Jackson, R.G. Welch, E.R. Palenque and S.B. Palmer, Measurement Sci. Technol. 6 (1995) 337.